Closed-form Inverse Kinematic Solution for Anthropomorphic Motion in Redundant Robot Arms

by

Yuting Wang

A Thesis Presented in Partial Fulfillment
of the Requirements for the Degree
Master of Science

Approved Novemberl 2013 by the
Graduate Supervisory Committee:

Panagiotis Artemiadis, Chair
Marc Mignolet
Veronica J. Santos

ARIZONA STATE UNIVERSITY

December 2013

ABSTRACT

As robots are increasingly migrating out of factories and research laboratories and into our everyday lives, they should move and act in environments designed for humans. For this reason, the need of anthropomorphic movements is of utmost importance. The objective of this thesis is to solve the inverse kinematics problem of redundant robot arms that results to anthropomorphic configurations. The swivel angle of the elbow was used as a human arm motion parameter for the robot arm to mimic. The swivel angle is defined as the rotation angle of the plane defined by the upper and lower arm around a virtual axis that connects the shoulder and wrist joints. Using kinematic data recorded from human subjects during every-day life tasks, the linear sensorimotor transformation model was validated and used to estimate the swivel angle, given the desired end-effector position. Defining the desired swivel angle simplifies the kinematic redundancy of the robot arm. The proposed method was tested with an anthropomorphic redundant robot arm and the computed motion profiles were compared to the ones of the human subjects. This thesis shows that the method computes anthropomorphic configurations for the robot arm, even if the robot arm has different link lengths than the human arm and starts its motion at random configurations.

ACKNOWLEDGEMENTS

I would like to express my sincere gratitude to my advisor, Dr. Artemiadis, for the continuous support throughout my Master's program, for his patience, motivation, enthusiasm, immense knowledge and the opportunity to work in the lab. I thank my fellow lab mates in the HORC lab for the stimulating discussions and for all the fun we have had in the last two years. Last but not the least, I would like to thank my parents for their love and support.

TABLE OF CONTENTS

LIST OF TABLES

LIST OF FIGURES

Chapter 1

INTRODUCTION

As the spectrum of application for robotic devices increases, the consideration of their configurations during interactions is essential. In certain complex industrial tasks, stable, fast and accurate robot positioning is required; while in a number of non-industrial tasks (e.g. domestic robotics, robotic-assisted surgery etc.) dexterity and intelligent positioning is required to avoid obstacles [21], joint limits [19] or singular configurations [23]. Robotic redundancy in manipulators usually solves these problems. However, the main difficulty of redundant robotic manipulators is that the task cannot define the joint motions uniquely. That is to say there is a superabundance of variables (joints) to position and orient the end effector. One attempt to solve this is to introduce kinematic and dynamic criteria. An alternate idea is to use the idea of human imitation. This concept is far removed from the initial design of robotic manipulators: factory oriented. Industrial robots have been used on manufacturing for a long time with their benefits to improve the quality and efficiency and replace human workers in tasks that may threaten human safety and health. Despite their rather long history, the physical presence of humans is still not allowed in the robot's workspace while it is working. On the other hand, service robotics have become a new and expanding area of robot application, such as home robotics. Therefore, there grows a fast interest in the humanoid robots supporting the expectations that the future robots will be required to work directly with human counterparts. Hence, they should feature human-like characteristics in their abilities and behavior especially in motion [28].

The investigation of human arm motion, in order to define a human model that leads to principles allowing more natural and effective interactions, has been thoroughly studied [27]. In [4], the hypothesis was demonstrated that it was possible to associate cost functions to each human arm joint and The arm performed movements that optimized these cost functions. Since then, a variety of methods similar to this have been used to

explain the principles of human arm motor control such as: dynamic principles [9, 10, 12], neuro-physiological and psychophysical [6,30,36], as well as combinations of those [4,17]. However, the majority of these cost functions are used with global optimization methods which are computationally expensive and not suitable for real-time implementation.

Human motion capture has been widely used for the generation of kinematic models describing human and humanoid robot motions [38]. There have been efforts to generate human-like motion by imitating the human arm as closely as possible [13]. Similarly, some works are based on minimizing posture differences between the robot and human arm, using a specific recorded data set [3,24]. Therefore, the robot configurations are exclusively based on the recorded data set. There are also some biomimetic approaches based on the dependencies among the human joint angles [1, 7]. In [7], the authors generalized the inverse kinematic solution by encompassing joint limitation, singularity avoidance and optimum manipulability measures. However, the proposed work requires the robot arm with similar structure and length of the human arm, while its iterative solution method is not efficient for real-time processing.

1.1 Motivation

The increasing demand of robots which can interact, communicate and collaborate with humans requires human-like behavior, which will allow the human subject to be able to understand the robot's intentions and seamlessly collaborate with the robot. Its application fields range widely from service robotics to therapeutic devices [7].

In order for the human-robot cooperation to be intuitive, the robot configurations should be anthropomorphic [2,28]. A solution to the inverse kinematic configuration of the manipulator must obey the constraints of anthropomorphism. This is not straightforward, since the human arm is redundant, i.e. it has 7 degrees of freedom (DOFs), while only 6 DOFs are required for a given position and orientation of the arm endpoint. This creates a challenge for the redundant robot inverse kinematics that need to be solved in a similar

way to that of the human arm, in order to guarantee seamless integration [14, 15, 22].

The scopes of previously proposed criteria are limited in several key areas while resolving the human arm redundancy and mimicking the human arm movements and those deficiencies suggest: (1) there is no full understanding of anthropomorphism; (2) most criteria are task dependent; (3) there exists high level computational cost and numerical instability problems. All of this calls for a new redundancy resolution criterion that is developed based on human arm kinematics data collected during a wide variety of daily activities. It also demands a control strategy that is not dependent on a robot structure identical to the human arm - since none exist or are immediately feasible. Therefore is must be applied to robot arms which have different structure and length from human arms. Moreover, it should be numerically stable and computationally efficient.

1.2 Objective

In this thesis, the problem of generating human-like motions is considered from the kinematic point of view, taking into account data recorded during a wide variety of everyday life tasks. A hypothesis from neurophysiology is applied for generating human-like motions of a redundant anthropomorphic robot arm. The human arm swivel angle (the rotation angle of the plane defined by the upper and lower arm around a virtual axis that connects the shoulder and wrist joints [15]) is used as a parameter for the robot arm to mimic, and therefore the problem of the inverse kinematics is simplified. A linear sensorimotor transformation model (see **Chapter 2**) is validated and used to estimate the desired swivel angle using previous knowledge of human arm motion. Finally the proposed controller's performance is evaluated on a 7 DOFs robot arm (LWR 4+, KUKA).

1.3 Overview

Chapter 2 explores the previous publications and studies related to this objective. In the beginning, the section reviews the benefits and applications of redundant structures. The next section introduces a few studies initiated towards studying the redundancy of the hu-

man arm and methods to infer laws for biomimetic robot inverse kinematics. **Chapter 3** introduces the proposed method for a closed-form inverse kinematic solution for anthropomorphic motion. It provides a thorough explanation of all stages of the methodology for the study. **Chapter 4** presents the demonstration of the linear sensorimotor transformation model maps the extrinsic coordinates on a natural arm posture using the intrinsic coordinates and performance estimation results of the swivel angle. It also provides a discussion on the results and method evaluation. Finally, **Chapter 5** summarizes the findings of the thesis and insight into continuing and future work.

Chapter 2

BACKGROUND LITERATURE

The exploitation of kinematic redundancy for the generation of human-like robot arm motions has been previously investigated. Since the method proposed in this thesis is based off from the evolving methods, it is important to review all these methods. Accordingly, this chapter begins with the methods employed previously. The approach to track the motion of the upper limbs, the study of the redundancy of the human arm and methods to infer laws for biomimetic robot inverse kinematics are discussed in the section that follows. The last section helps give context to the rationale of this thesis.

2.1 Introduction

From a mechanical point of view, a robot resembling the human should be kinematically redundant, i.e., its mechanism should possess a higher degree of mobility than that required for a given motion task defined in operational space. The kinematic redundancy contributes to robot dexterity and flexible coping with unpredictable changes in its environment [28]. It makes possible the avoidance of mechanical limits in robot joints [19], the avoidance of obstacles [21], the avoidance of singularities [41], a fault tolerant operation [8], the optimization of robot kinematics and dynamics [11, 42], the distribution of joint motions in a human-like manner [25] and so on. Unfortunately, redundancy usually causes the problem of complex kinematics. Since their joint configuration is not determined uniquely, a set of kinematic and dynamic criteria have been introduced to achieve a unique solution. During the last decade though, the robots are getting closer to humans, thus introducing the need for anthropomorphic motion to allow improved interaction. Towards this goal, the investigation of human arm motion has been reported in the past, including approaches of mimicking the human arm movements, cost functions to model motion principles of human arm movements. Again, all the previously proposed criteria have shown that they have limitations in resolving the human arm redundancy and mimicking the human arm

movements.

2.2 Kinematic Redundancy

Redundant robots have received increased attention during the last decades in order to avoid obstacles, joint limits, or to optimize robot kinematics and dynamics. Maciejewski [21] presented work to determine the required joint angle rates for the manipulator under the constraints of multiple goals, the primary goal described by the specified end-effector trajectory and secondary goals describing the obstacle avoidance criteria. The decomposition of the solution into a particular and a homogeneous component effectively illustrates the priority of the multiple goals that was exact end-effector control with redundant degrees of freedom maximizing the distance to obstacles. In [19], Alain proposed a two-level adaptive control of the redundant kinematics of multi-body mechanisms. A special form of the general solution of sets of linear equations was used and the adaptive qualities of a six DOF manipulator illustrated the theoretical results. In [11], two different types of methods for resolving kinematic redundancies of manipulators by the effect on joint torque were examined. One method chose the joint acceleration null-space vector to minimize joint torque in a least squares sense while contrasting methods employing only the pseudo-inverse with and without weighting by the inertia matrix. The results showed an unexpected stability problem during long trajectories for the null-space methods and for the inertia-weighted pseudo-inverse method, but more seldom for the unweighted pseudo-inverse method. Evidently, a whiplash action developed over time that thrust the endpoint off the intended path, and extremely high torques were required to overcome these natural movement dynamics.

2.3 Classical Methods to Resolve Redundancy

The presence of a higher degree of mobility in the robot mechanism, than is required for a given motion in operational space means that the same end-effector's trajectory can be realized with many different configuration motions. Hence, the problem of selecting a particular motion among the available joint motions arises. The standard methods to deal with this problem are divided into two groups, i.e., global and local methods. The global

methods require the prior knowledge about the full end-effector's trajectory, since they look for joint motions that provide the global optimum of the adopted criterion. On the contrary, local methods perform only local optimization of the criterion and need only information about the instantaneous pose of the end-effector. For on-line robot operation and especially in the physical presence of humans, local methods for redundancy resolution are required [28]. Therefore, the local methods are more applicable in controlling the robot manipulators. In [26, 28], a distributed positioning method was used by partitioning of the robot joints into "smooth" and "accelerated" ones in order to achieve human-like motion. The method was applied to control the motion of a redundant anthropomorphic arm during the writing task. The reason for the usual inclination of letters in human handwriting was revealed and the relation between the inclination, legibility and certain secondary objectives (fingers' involvement, energy consumption and motors' thermal load) was discussed. It was shown that for some prescribed level of legibility, there exists an optimal inclination that minimizes the secondary objective.

2.4 Bio-inspired Methods to Resolve Redundancy

For everyday life tasks (e.g. drawing, handwriting), approaches of mimicking the human arm movements have been proposed. Some studies have been also done in order to generate human-like motion by imitating human arm motion as closely as possible. In most of these studies, the human motion is measured using a motion capture system and then converted to motion for a humanoid robot arm [24]. In [13], a method was proposed to convert the captured marker data of human arm motions to robot motion using an optimization scheme. The position and orientation of the human hand, along with the orientation of the upper arm, were imitated by a humanoid robot arm. However, this method was not able to generate human like motions, given a desired three dimensional (3D) position for the robot end-effector. Again, previous research like this can not generate new human-like motion, which is quite important for the kinematic control of anthropomorphic robot arms and humanoids, where the range of possible configurations should not be limited to

the ones recorded from humans. Cost functions have also been proposed to model motion principles of human arm movements. In [5], an investigation was conducted to look for measurable values corresponding to the hypothetical cost functions and conclusion were made that the hypothetical cost functions were not independent of the physiological costs necessary to hold the joint at a given angle, and they seemed to depend on joint angle and on the force which is necessary to hold the joint in a given position. However, these functions are quite complex to be used for the inverse kinematics of robots, while they are usually addressing not only the kinematic, but also manipulator dynamics and kinetics. Biomimetic approaches based on the dependencies of the joint angles were applied in the inverse kinematics algorithms [1, 7]. In [1], the human arm multi-joint coordination was analyzed in order to synthesize motion patterns for robot arms. A Bayesian Network was used for the probabilistic description of the human arm multi-joint coordination. Then an objective function was defined based on the inter-joint dependency, which was incorporated into a closed-loop inverse kinematics algorithm for a redundant robot arm. However, in [7], the proposed method requires the robot arm with similar structure of the human arm. Also its iterative solution method is not efficient for real-time processing and in [1], even though its method can be applied to a robot arm with different structures from that of human arms, it is still difficult to build the relationship between the human and robot joints.

2.5 Redundant Degree of Freedom: Swivel Angle

As shown in Fig. 2.1, a simple physical explanation of the redundant degree of freedom is based on the observation that if the wrist is held fixed, the elbow can still swivel along a circle plane which is perpendicular to the axis from the shoulder to the wrist [37, 40]. Therefore, for a fixed position of the shoulder in space, along with a given position and orientation of the wrist, the human arm configuration is fully defined if and only if the position of the elbow joint is fully specified [15].

The workspace of this structure was first methodically analyzed by Korein [16]. He observed that the first two shoulder joints restrict the tip of the elbow to lie on a spherical

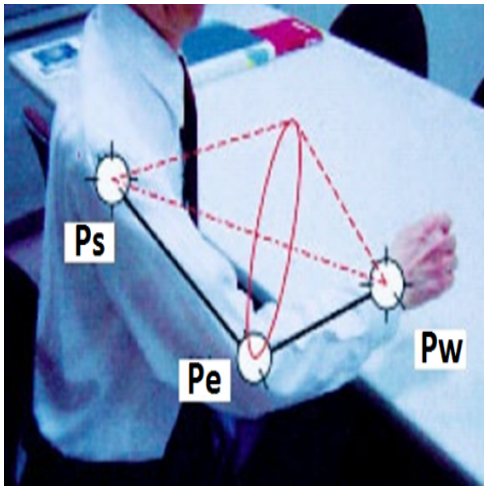

Figure 2.1: From [40], the explanation of the human arm redundancy. Even after fixing the hand position and orientation, the elbow can move along a part of the circle shown in the figure, implying that the arm has one redundant degree of freedom.

plane. The potential elbow configurations was determined by the joint limits of the first two joints by intersecting the elbow circle with the plane. In addition to the joint limits, the twist induced by the third joint also restricts the elbow to lie on a circular plane which is perpendicular to the axis from the shoulder to the wrist. On the other hand, the wrist joints will also restrain the elbow position along with their joint limits. By taking the intersection of all sets of valid elbow arcs, Korein derived the restrictions on the elbow position induced by all the joint limits.

Another approach to solving this problem is based on the same observation as Korein's. It gives an explicit formula for the joint angles and their derivatives as a function of the swivel angle (ϕ). This is an advantage when an objective function is used to select an appropriate value of ϕ since it is often necessary to express the objective function in terms of the joint angles. In Fig. 2.2, $\mathbf{P_s}$, $\mathbf{P_e}$ and $\mathbf{P_w}$ represent the position of the shoulder, the elbow, and the computed location of the wrist based on the given position and orientation of the end effector. As the swivel angle ϕ varies, the elbow traces an arc of a circle lying on a plane which is perpendicular to the wrist-to-shoulder axis. In order to measure ϕ, we define the normal vector of the plane by the unit vector in the direction from the shoulder

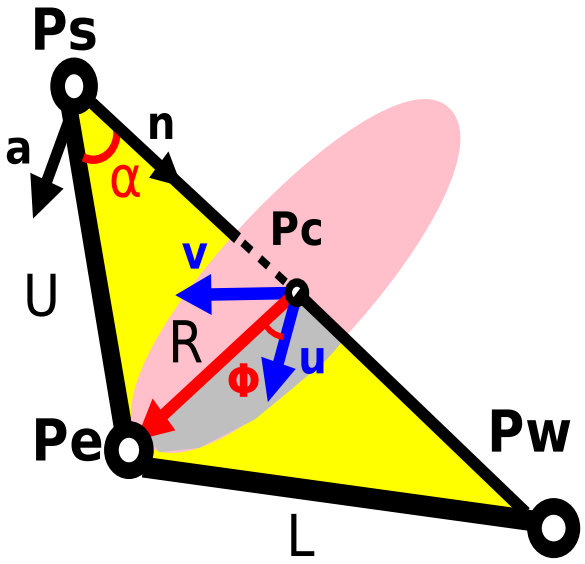

Figure 2.2: Coordinate frame at the center of the elbow circle and the swivel angle that allows the parametrizations of the elbow position by a single variable.

to the wrist,

$$\tilde{\mathbf{n}} = \frac{\mathbf{P_w} - \mathbf{P_s}}{\| \mathbf{P_w} - \mathbf{P_s} \|} \tag{2.1}$$

$\mathbf{P_c}$ as the center of the circle and unit vector $\tilde{\mathbf{u}}$, $\tilde{\mathbf{v}}$ as the coordinate system on the plane. $\tilde{\mathbf{u}}$ is set as the projection of an arbitrary axis $\tilde{\mathbf{a}}$ onto the plane of the circle,

$$\tilde{\mathbf{u}} = \frac{\tilde{\mathbf{a}} - (\tilde{\mathbf{a}} \bullet \tilde{\mathbf{n}})}{\| \tilde{\mathbf{a}} - (\tilde{\mathbf{a}} \bullet \tilde{\mathbf{n}}) \|} \tag{2.2}$$

and $\tilde{\mathbf{v}}$=$\tilde{\mathbf{n}} \times \tilde{\mathbf{u}}$. The center of the circle $\mathbf{P_c}$ and its radius R can be computed from simple trigonometry:

$$cos(\alpha) = \frac{\| \mathbf{P_w} - \mathbf{P_s} \|^2 + U^2 - L^2}{\| \mathbf{P_w} - \mathbf{P_s} \| U} \tag{2.3}$$

$$\mathbf{P_c} = cos(\alpha) U \tilde{\mathbf{n}} \tag{2.4}$$

$$R = sin(\alpha) U \tag{2.5}$$

where U and L are the length of the upper arm and the lower arm respectively.

Finally, the position of the elbow can be expressed as a function of ϕ such that,

$$\mathbf{P_e} = R[\cos(\phi)\tilde{\mathbf{u}} + \sin(\phi)\tilde{\mathbf{v}}] + \mathbf{P_c} \tag{2.6}$$

2.6 Velocity Manipulability Ellipsoid and Redundancy

For the combined manipulator joint velocities satisfying the condition stated as $\sum_{i=1}^{n} \dot{\theta}_i^2 = 1$, the end effector velocity as a function of the arm joint velocity is described by an ellipsoid known as the velocity manipulability ellipsoid [15]. The orientation of the ellipsoid with its three major axes is defined by the eigenvectors of the Jacobian and the lengths of the major axes are defined by the eigenvalues of the Jacobian [18]. The largest among the major axes of the manipulability ellipsoid defines the direction of the highest potential for velocity on the wrist and the best mapping between the arm joint space and the wrist Cartesian space [20].

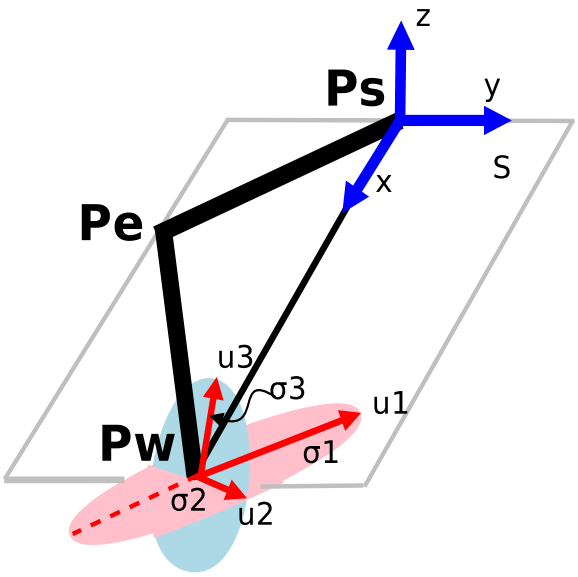

Figure 2.3: New coordinate system composed of $\mathbf{P_w}$, $\mathbf{P_e}$, $\mathbf{P_s}$ where x-axis is defined as a unit vector along $(\mathbf{P_w} - \mathbf{P_s})$ and y-axis sits on the plane S. The new frame on the shoulder is defined for the convenience of the calculation. Manipulability ellipsoid on the wrist position: $\mathbf{u_1}$, $\mathbf{u_2}$, and $\mathbf{u_3}$ indicate the three major axes of the ellipsoid with magnitude of σ_1, σ_2, and σ_3.

In [15], the longest axis of the manipulability ellipsoid is aligned along plane S (shown in Fig. 2.3) and its magnitude σ_1 (defined by the largest eigenvalue of Jacobian, λ_1) and direction $\mathbf{u_1}$ (defined by the eigenvector of Jacobian) were both expressed as a function of the swivel angel (ϕ), the length of the lower arm (L) and the distance from the

wrist to the shoulder (L_{ws}).

$$\sigma_1 = \sqrt{\lambda_1} = \sqrt{\frac{(c_1+1)({L_{ws}}^2+L^2)}{2}} \tag{2.7}$$

$$c_1 = \frac{\sqrt{({L_{ws}}^2+L^2)^2 - 4{L_{ws}}^2 L^2 sin(\phi)^2}}{{L_{ws}}^2+L^2} \tag{2.8}$$

$$\mathbf{u_1} = \begin{bmatrix} 1 \\ -\dfrac{\lambda_1}{L^2 sin(\phi)^2} - \dfrac{1}{tan(\phi)} \\ 0 \end{bmatrix} \tag{2.9}$$

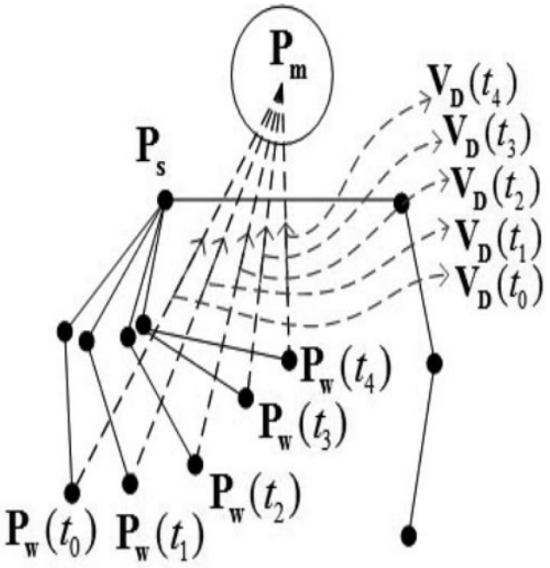

Figure 2.4: From [15]: graphical representation of its redundancy resolution criterion indicating that for the given wrist position ($P_w(t_i)$) at any given time t_i, there is a virtual path ($V_D(t_i)$) toward the subjects' heads (P_m), where $i = 0, 1, 2, 3 \cdots$.

From equations above, it's easy to see that $\mathbf{u_1}$ always lies on Plane S. The report [15] hypothesized that, for the natural reaching and grasping tasks, the value of swivel angel selected by human motor control system to resolve the arm redundancy should be selected to efficiently retract the palm to the head. Therefore, there should exist a virtual target point ($\mathbf{P_m}$) on the head that was set to efficiently retract the palm to the virtual target at any time during the arm movement toward an actual target (shown in Fig. 2.4). Mathematically speaking, the selected swivel angle for the natural arm posture was chosen in a way that

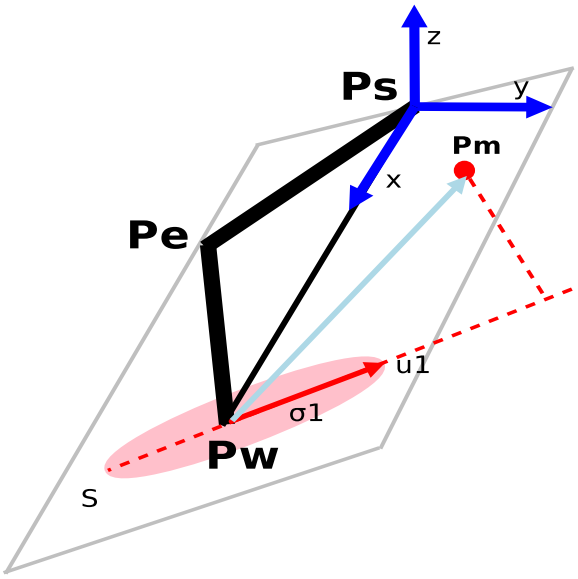

Figure 2.5: It shows the specific elbow position for the given wrist position that maximizes the manipulability projected on the virtual trajectory. In this configuration $\mathbf{P_m}$, $\mathbf{P_s}$, $\mathbf{P_e}$ and $\mathbf{P_w}$ are on the same plane.

the projection of the longest axis of the manipulability ellipsoid onto the virtual trajectory ($\mathbf{P_m} - \mathbf{P_w}$) was maximized. Based on Eq. 2.7, 2.8, 2.9, it is easy to prove that the projection is maximized when ϕ is selected such that $\mathbf{P_m}$ locates on Plane S shown in Fig. 2.5. Fig. 2.6 shows the real time trajectory of $\mathbf{P_m}$ with respect to the right arm shoulder position. It appears that the trajectory was around the head region but the actual $\mathbf{P_m}$ was not identical for each trial. More importantly, this hypothesis has a problem that the tasks for the subjects are limited to simple reaching and grasping and there is no proof that it can be applied to more complicated tasks such as writing. Also, the method to solve the inverse kinematic problem requires the initial configuration of the human arm to be known, a feature that is not readily available in real-life scenarios.

2.7 Linear Sensorimotor Transformation Model

In order to understand the secret of human arm movements, Soechting [33, 34] defined an extrinsic frame of reference to represent the location of a point relative to a human subject's shoulder, and an intrinsic frame of reference to represent the orientation of the arm and forearm. Then the relationships between those two reference coordinates was examined

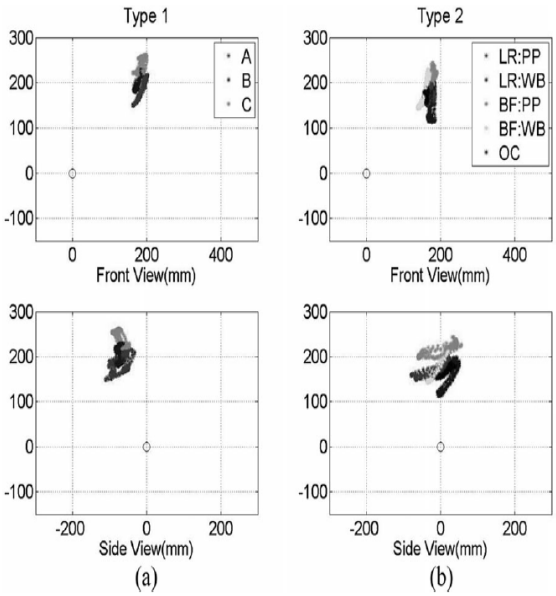

Figure 2.6: From [15]: (a) and (b) shows exemplary plots of $\mathbf{P_m}(t)$ for all task types from one subject. Upper and lower rows indicate the front and side views of (looking at the right shoulder) Pm with respect to the shoulder (reference frame) in millimeter scale. Black empty circles indicate the right arm shoulder position $\mathbf{P_{sh}}$. $\mathbf{P_m}$ is individually estimated for each experiment and marked as a different color depending on the task type.

and proposed. It was concluded that this transformation was one step in the process of transforming a visually derived representation of target location into an appropriate pattern of muscle activity. From the measured position of the shoulder, elbow, and wrist, the orientation angles of the arm and forearm were computed (shown in Fig. 2.7). Two angles define the orientation of the upper arm: yaw (η) and elevation (θ), and two more define the orientation of the forearm: yaw (α) and elevation (β). The elevations (θ and β) define the angles between each limb segment and the vertical axis and are measured in a vertical plane. The yaw angles (η and α) define the angles between each of the limb segments and the anterior direction, measured in the horizontal plane. The extrinsic coordinates are the wrist position expressed in the spherical coordinates, where R denotes the radial distance, χ the azimuth, and ψ the elevation. The reason to choose the spherical coordinates rather than Cartesian or cylindrical is the former leads to a more compact representation of the linear relation [35]. Both the intrinsic and extrinsic coordinates are most easily defined

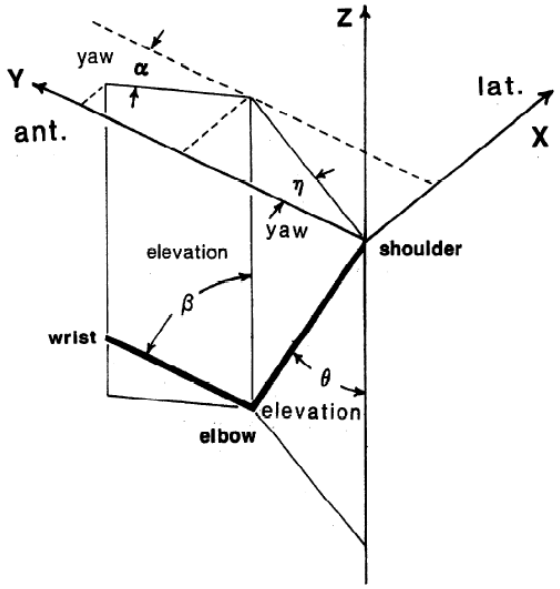

Figure 2.7: From [34]: Orientation angles of the arm and forearm. The angles θ and η define the elevation and the yaw of the upper arm and β and α represent the elevation and yaw of the forearm. Elevation is defined as the angle between the limb segment and the vertical axis and is measured in a vertical plane. Yaw is the angle between the limb segment and the anterior direction, measured in the horizontal plane.

with reference to the Cartesian coordinates illustrated in Fig. 2.7. The relationship between these two coordinates can be easily found:

$$P_w(x) = Usin(\theta)sin(\eta) + Lsin(\beta)sin(\alpha) \tag{2.10}$$

$$P_w(y) = Usin(\theta)cos(\eta) + Lsin(\beta)cos(\alpha) \tag{2.11}$$

$$P_w(z) = -Ucos(\theta) + Lcos(\beta) \tag{2.12}$$

where $P_w(x)$, $P_w(y)$ and $P_w(z)$ designate the Cartesian components of the wrist position with respect to the shoulder frame. U and L represent the length of the upper arm and the lower arm.

The wrist position in the Cartesian coordinates can be transformed to the spherical coordinates by:

$$R^2 = P_w(x)^2 + P_w(y)^2 + P_w(z)^2 \tag{2.13}$$

$$tan(\chi) = \frac{P_w(z)}{-P_w(y)} \tag{2.14}$$

Table 2.1: From [33]: Linear relationship between the intrinsic and extrinsic coordinates

i	$OrientationAngles$	$LinearFunction$	r^2
1	θ	$0.110R+0.9\psi-4$	0.88
2	η	$0.056R+0.79\chi+52.6$	0.91
3	α	$-0.021R+0.96\chi+8$	0.94
4	β	$0.033R-0.95\psi+47.6$	0.86

$$tan(\psi) = \frac{P_w(x)}{\sqrt{P_w(y)^2 + P_w(z)^2}} \tag{2.15}$$

To understand the nature of the transformation between extrinsic and intrinsic coordinates in the two motor tasks, Soechting characterized quantitatively how each of the intrinsic parameters depend on each of the extrinsic variables. They examined this under two experimental conditions: 1) pointing to a virtual target in the dark and 2) pointing to a target which was physically present and both it and the arm were visible to the subjects. They found that when subjects pointed to a virtual target in the dark, each of the four intrinsic parameters which describe the orientation of the arm and forearm (θ, η, α, β) depended in a close to linear fashion on one or two of the extrinsic parameters which describe the spatial location of the target (R, χ, ψ). Table 2.1 shows the results from their experiments. As shown in Table 2.1, the two elevation angles (θ and β) depend on target distance (R) and elevation (ψ), whereas the two yaw angles (η and α) depend primarily on target azimuth (χ) with a weaker dependence on ψ. When subjects made accurate movements to a target, these relationships between intrinsic and extrinsic coordinates became significantly more nonlinear. This conclusion was supported by the combined data from all four subjects in each experimental condition.

Based on the observation, the following hypotheses were derived in [34]: movement inaccuracy results because the subjects map the target location into the space of intrinsic parameters, and this mapping involves quasi-linear approximations. Accurate movements appeal to corrections which introduce substantial nonlinearities into the relationship be-

tween intrinsic and extrinsic parameters. Their hypotheses were strengthened by results in [31, 32, 39]. Thus, there is experimental evidence that is consistent with this hypothesis that there exist linear mappings between extrinsic and intrinsic coordinates both for continuous as well as for point-to-point movements. Furthermore, such linear mappings can account for the observed movement errors. Therefore, the assumption that coordinated movement involves sensorimotor transformations between different kinematic representations (intrinsic and extrinsic) and the hypothesis that these transformations are accomplished by means of linear approximations can account for the performance of a large variety of motor tasks. Despite the fact that it needs the robot arm to have a similar arm length with that of the human arm, it still provides a good mathematical quantification of anthropomorphism with no limitation on the robot arm structure (as long as the upper and lower arm are well defined). Furthermore, this linear relationship can give us good estimations for the orientation angles and the elbow and wrist positions are simply a function of those orientation angles. Knowing the elbow and wrist positions, it is easy to obtain a unique inverse kinematic solution for the joint angles. Therefore, this method offers an analytical solution for the joint angles, which can avoid the high level computational cost for real-time implementation into control systems.

Chapter 3

METHODOLOGY

This chapter presents the full framework for solving the inverse kinematics problem of redundant robot arms that results to anthropomorphic configurations. As mentioned in **Chapter 2**, Soechting [33, 34] demonstrated a linear sensorimotor transformation model that maps the extrinsic coordinates on a natural arm posture using the intrinsic coordinates providing a mathematical description of anthropomorphism for human arm motions. There is also experimental evidence showing that this linear mapping exists for both continuous and point to point movements. Therefore, their theory can account for a large variety of motor tasks even though only one simple task was validated in their report. However, it requires the length of the robot arm similar to that of the human arm. Because the linear relationship is a function of the arm length, the large difference will affect the estimation results.

As discussed in **Chapter 2**, the swivel angle was considered as a main factor to quantify the redundancy. The swivel angle concept has already been used by many studies [14, 15, 22, 37]. In [15], the relationship between the swivel angle and the velocity manipulability ellipsoid of the wrist was analyzed and the swivel angle was selected such that the projection of the largest manipulability vector onto the virtual trajectory connecting the wrist with the head region is maximized. Even though this method has its limitation in the application on more complex tasks and the requirements for initial configurations for the human arm, it still contributed a relationship between the swivel angle and the longest axis of the velocity manipulability ellipsoid (see Eq. 2.7, 2.8, 2.9). This gives a way to quantify the anthropomorphism of the robot arm configuration based on a given human arm posture: the swivel angle of the robot arm should be as close as possible to that of the human. Here it should be noted that it will set us free from the requirements for the length and structure of the robot arm.

Table 3.1: Human Arm D-H Parameters

i	α_i	a_i	d_i	θ_i
1	90°	0	0	q_1
2	90°	0	0	$q_2 + 90^\circ$
3	90°	0	L_1	$q_3 + 90^\circ$
4	90°	0	0	$q_4 + 180^\circ$
5	90°	0	L_2	$q_5 + 180^\circ$
6	90°	0	0	$q_6 + 90^\circ$
7	90°	L_3	0	$q_7 + 180^\circ$

Although most of the past studies have been trying to quantify anthropomorphism, most works on biomimetic motion generation for robots are based on minimizing posture difference between the robot and the human arm, using a specific recorded data set and there are only a handful studies that focused on defining the foundation rules of the human arm motion which still have limitations. This proposed method will combine those two methods mentioned above in order to obtain an anthropomorphic solution for the inverse kinematic of 7-DoF robot arm given the position and orientation of the end-effector.

3.1 Human Arm Kinematics

As it shown in Fig. 3.1, the human arm consists of a series of rigid links connected by three anatomical joints (shoulder joint, elbow joint, and wrist joint) while neglecting the scapular and clavicle motions [16]. In this study, 7 DOFs were analyzed for simplicity: shoulder flexion-extension, shoulder abduction-adduction, shoulder lateral-medial rotation, elbow flexion-extension, elbow pronation-supination, wrist flexion-extension and wrist pronation-supination: which can be simulated by 7 corresponding joint angles, i.e. q_1, q_2, q_3, q_4, q_5, q_6, q_7 for the human arm. The Denavit-Hartenberg (DH) parameters of the kinematic model of the arm that we used are listed in Table 3.1 [7, 29] where L_1, L_2, L_3 are the lengths of the upper arm, forearm and palm respectively[1].

[1] Offsets in θ_i are used for having the arm at rest position (pointing down) when $q_i = 0, i = 1, \ldots 7$.

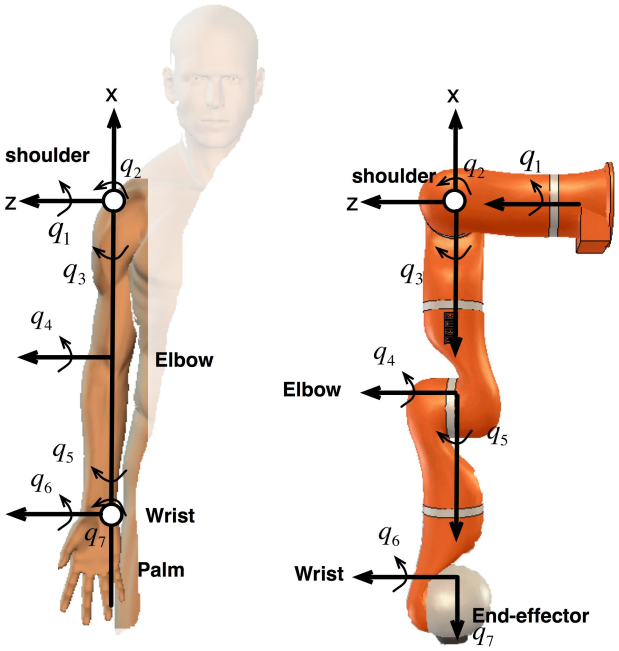

Figure 3.1: Kinematic models of the human and robot arms.

Table 3.2: LWR4+ KUKA Arm Model D-H parameters

i	α_i	a_i	d_i	θ_i
1	90°	0	0	q_1
2	90°	0	0	q_2
3	90°	0	L_u	q_3
4	90°	0	0	q_4
5	90°	0	L_f	q_5
6	90°	0	0	q_6
7	0°	0	L_h	q_7

3.2 Robot Arm Model

Fig. 3.1 also shows the reference and link coordinate systems of the 7 DOFs robot arm (LWR4+, KUKA) using the DH convention [29]. The values of the DH parameters are listed in Table 3.2, where L_u, L_f and L_h are the link lengths of robot upper-arm, forearm and hand respectively. There are several differences between the human arm and the robot arm:

1. The human arm has a spherical wrist (q_5, q_6 and q_7 axes intersect at a single point) while the robot arm does not.

2. The length of the LWR4+ KUKA arm is almost twice as much as that of the human arm.

3.3 Reduction of Joint Variables

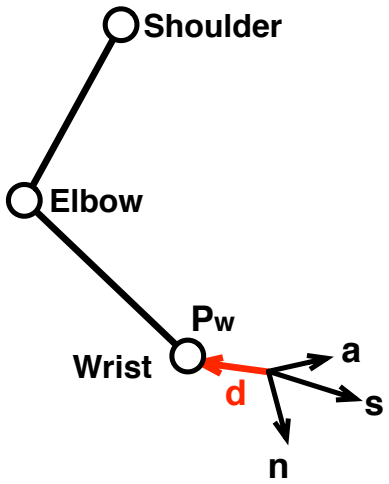

Figure 3.2: Wrist position with respect to the end-effector frame

For a given position and orientation of the end-effector with respect to the base frame, the wrist position can be easily defined. As shown in Fig. 3.2, once the end-effector position and orientation are specified in terms of $\mathbf{p_{ee}}$ and $\mathbf{R_{ee}}=\begin{bmatrix} \mathbf{n} & \mathbf{s} & \mathbf{a} \end{bmatrix}$, the homogeneous transformation relating the description a point in the end-effector frame to the description of the same point in base frame can be represented as

$$\mathbf{T_e^b} = \begin{bmatrix} \mathbf{n} & \mathbf{s} & \mathbf{a} & \mathbf{p_{ee}} \\ 0 & 0 & 0 & 1 \end{bmatrix} \tag{3.1}$$

then the wrist position in the end-effector frame can be represented as

$$\mathbf{P_{we}} = \begin{bmatrix} d_x \\ d_y \\ d_z \end{bmatrix} \tag{3.2}$$

where d_x, d_y, d_z are the coordinates of the wrist center with respect to the origin of the end-effector frame.

This allows direct computation of the wrist position with respect to the base frame given the end-effector frame [29]. In our case, the base frame is located at the center of the shoulder for both arm models shown in Fig. 3.1. The position of the wrist $\mathbf{P_w}$ in the base frame can be found as:

$$\begin{bmatrix} \mathbf{P_w} \\ 1 \end{bmatrix} = \mathbf{T_e^b} \begin{bmatrix} \mathbf{P_{we}} \\ 1 \end{bmatrix} \tag{3.3}$$

Given a desired position and orientation of the end-effector, the problem is split into two parts:

1. Using Eq. 3.3 compute the wrist position: since the wrist position is only a function of the first 4 joint angles (q_1-q_4) we define a method to solve for those joints. This step involves redundancy in joint angles and it is going to be solved in a way to guarantee anthropomorphism (see *Redundancy resolution* section).

2. Knowing q_1-q_4 and the desired position and orientation of the end-effector frame, analytically solve for q_5-q_7. Therefore, the structure difference of these two arms can be neglected.

3.4 Redundancy Resolution
Quantify Anthropomorphism For The Robot Arm

There is evidence from previous works that the position of the elbow joint in space is an important parameter of anthropomorphism for arm configurations [2, 15]. In [15, 37], the redundancy of the arm was formulated by defining the swivel angle, the rotation angle of the plane defined by the upper and lower arm around a virtual axis that connects the shoulder and wrist joints. The position of the elbow can be expressed as a function of the swivel angle by Eq. 2.6. It was also mathematically proven that the direction and the magnitude of the longest axis of the velocity manipulability ellipsoid of the wrist is

simply a function of the swivel angle and the arm length. As shown in Fig. 3.3, $\mathbf{u_1'}$ and σ_1' represent the direction and magnitude of the longest axis of the velocity manipulability ellipsoid on the wrist for the robot arm. $\mathbf{P_s'}$ and $\mathbf{P_e'}$ represent the shoulder and elbow position for the robot arm and P_s and P_e represent the shoulder and elbow position for the human arm. Here it should be noted that P_s and P_s' coincide. The projection of $\mathbf{u_1'}$ onto $\mathbf{u_1}$ can be maximized if and only if $\mathbf{u_1'}$ is located on Plane S (Plane S is formed by the shoulder, elbow and position of the human arm.) which is determined by the swivel angle with a given wrist position (see proof in [15]). Therefore, the swivel angle of the robot arm should be chosen as close as possible to that of the human arm as they both seek to achieve maximization of manipulability ellipsoids for a given task. This method will not be constrained by the limitation of the difference of the arm structure and length as long as an elbow-equivalent point is defined on the robot arm. Once the value of the swivel angle is determined, the elbow position can be computed by Eq. 2.6. With the positions of the wrist and elbow, as well at the 3D position and orientation of the rigid body of the end effector, we are able to analytically give a unique solution to the inverse kinematic problem, and therefore compute the 7 joint angles of the upper limb.

Swivel Angle Estimation

Based on the linear sensorimotor transformation model discussed in **Chapter 2**, the orientation angles of the upper arm and the forearm can be obtained only knowing the wrist position. From the measured position of the shoulder, elbow, and wrist, the orientation angles of the arm and forearm were computed (shown in Fig. 3.4). Here it should be noted that, due to the convenience of the calculation, the way to set the base reference frame coincident with the base frame located on the center of the human shoulder which is different from that in Fig. 2.7. The intrinsic coordinates consist of angles defined the upper arm elevation and yaw and the forearm elevation and yaw. Two angles define the orientation of the upper arm: yaw (η) and elevation (θ), and two more define the orientation of the forearm: yaw (α) and elevation (β). The elevations (θ and β) define the angles between each

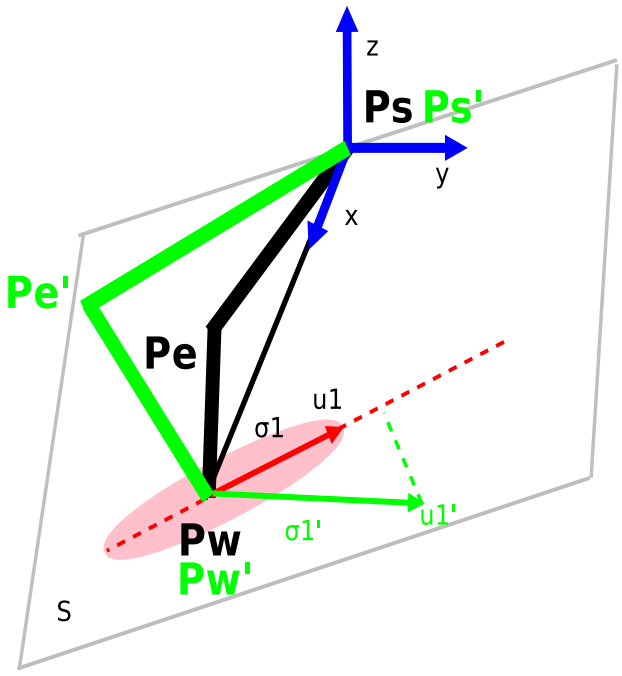

Figure 3.3: It shows the specific elbow position for the given wrist position that maximizes the manipulability projected on the virtual trajectory. In this configuration $\mathbf{P_m}$, $\mathbf{P_s}$, $\mathbf{P_e}$ and $\mathbf{P_w}$ for both the human and robot arm are on the same plane.

limb segment and the vertical axis and are measured in a vertical plane. The yaw angles (η and α) define the angles between each of the limb segments and the anterior direction, measured in the horizontal plane.The extrinsic coordinates are the wrist position expressed in the spherical coordinates, where R denotes the radial distance, χ the azimuth, and ψ the elevation. Therefore, as is shown in Fig. 3.4, the elbow position in this coordinate system can be expressed as:

$$P_e(x) = -Ucos(\theta) \tag{3.4}$$

$$P_e(y) = -Usin(\theta)cos(\eta) \tag{3.5}$$

$$P_e(z) = Usin(\theta)sin(\eta) \tag{3.6}$$

Where $P_e(x)$, $P_e(y)$ and $P_e(z)$ designate the components of the elbow position with respect to the shoulder frame. U represents the length of the upper arm.

The swivel angle can be obtained knowing the elbow position (computed by Eq. 3.4, 3.5, 3.6) and wrist position (computed by Eq. 2.10, 2.11, 2.12). Finally, the swivel

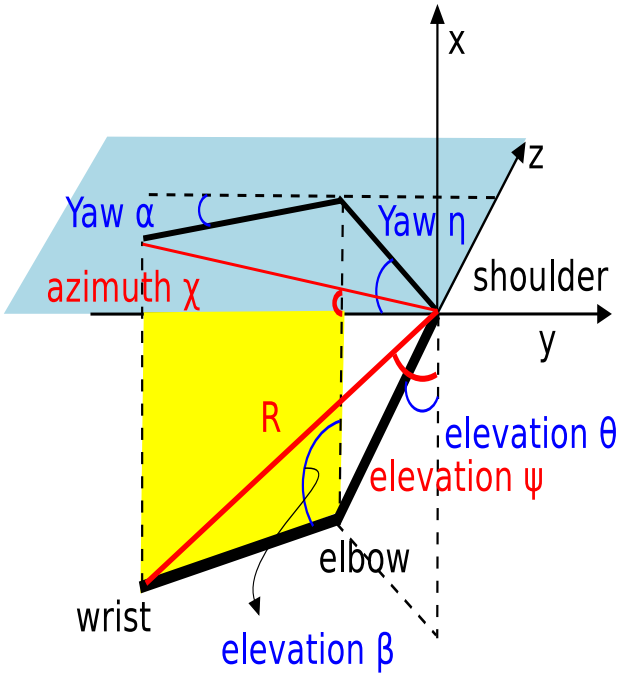

Figure 3.4: Orientation angles of the arm and forearm. The angles θ and η define the elevation and the yaw of the upper arm and β and α represent the elevation and yaw of the forearm. Elevation is defined as the angle between the limb segment and the vertical axis and is measured in a vertical plane. Yaw is the angle between the limb segment and the anterior direction, measured in the horizontal plane.

angle is selected using (Eq. 2.6):

$$\phi = atan2(\frac{(\mathbf{P_e} - \mathbf{P_c}) \cdot \vec{\mathbf{u}}}{\| \mathbf{P_e} - \mathbf{P_c} \|}, \frac{(\mathbf{P_e} - \mathbf{P_c}) \cdot \vec{\mathbf{v}}}{\| \mathbf{P_e} - \mathbf{P_c} \|}) \tag{3.7}$$

where $\mathbf{P_e}$ represents the elbow position, unit vector $\tilde{\mathbf{u}}$, $\tilde{\mathbf{v}}$ as the coordinate system on the plane shown in Fig. 2.2 and $\mathbf{P_c}$ is the origin of the coordinate system.

3.5 Wrist Position Correction

Since the sensorimotor transformation model is only an approximation, the wrist position given by the determined angles θ, η, α, β does not exactly coincide with the target one. However, the difference between the actual wrist position and the estimated is relatively small. Therefore, the error will not have big affect on the linear relationship. We can simply correct the wrist position with minimum change for each joint so that the human arm configuration will still approach to the linear transformation model while maintaining the correct wrist position. Let $\mathbf{e}$ represents the difference between the actual wrist position and

the estimated one (3×1 vector), $\mathbf{J}$ the Jacobian based on the estimated arm configuration ($\mathbf{J}$ is only a function of q_1, q_2, q_3 and q_4, a 3×4 matrix), $\delta\mathbf{q}$ the change of the joint angles (4×1 vector, only q_1, q_2, q_3 and q_4 are needed here), then

$$\delta\mathbf{q} = \mathbf{J}^{\dagger}(q_1, q_2, q_3, q_4)\mathbf{e} \tag{3.8}$$

$$\mathbf{q_u} = \mathbf{q} + \delta\mathbf{q} \tag{3.9}$$

where $\mathbf{q}$ is the current estimation for q_1, q_2, q_3 and q_4; $\mathbf{q_u}$ is the estimation for those joint angles after correction; $\mathbf{J}^{\dagger}$ is pseudo inverse of J.

Here it should be noted that all these joint angles are the estimation for the human model. After the correction of the joint angles, the updated elbow and wrist position can be obtained with forward kinematic and the swivel angle can be revised using Eq. 3.7. Once the swivel angle of the human is obtained, the elbow position for the robot arm can be computed by Eq. 2.6 (set the swivel angle of the robot arm equal to that of the human) and the wrist position of the robot arm can be computed by Eq. 3.3. With computed the elbow and wrist position of the robot arm and the location of the end-effector (given), a unique solution for all the joint angles can be obtained.

3.6 Solution for Inverse Kinematic Problem

Let $\mathbf{p_e} = \begin{bmatrix} x_e & y_e & z_e \end{bmatrix}^T$, $\mathbf{p_w} = \begin{bmatrix} x_w & y_w & z_w \end{bmatrix}^T$ be the position of the elbow and wrist with respect to the base frame. The position of the elbow is computed by Eq. 2.6, with the estimation of the swivel angle, using Eq. 3.7. The position of the wrist is computed using Eq. 3.3. Let the desired position and orientation of the end-effector be given by

$$\mathbf{T} = \begin{bmatrix} \mathbf{n_d} & \mathbf{s_d} & \mathbf{a_d} & \mathbf{p_d} \\ 0 & 0 & 0 & 1 \end{bmatrix}. \tag{3.10}$$

Since the position of the wrist and elbow are computed, then the solution for the first 4 joint angles has a closed form which is shown below:

$$q_1 = arctan2(y_e, x_e) \tag{3.11}$$

$$q_2 = arctan2(\sqrt{(x_e)^2 + (y_e)^2}, z_e) \tag{3.12}$$

$$q_3 = arctan2(-M_3, M_1) \tag{3.13}$$

$$q_4 = arctan2(\sqrt{(M_1)^2 + (M_3)^2}, M_2 - L_1) \tag{3.14}$$

where

$$M_1 = x_w \cos(q_1)\cos(q_2) + y_w \sin(q_1)\cos(q_2) - z_w \sin(q_2) \tag{3.15}$$

$$M_2 = -x_w \cos(q_1)\sin(q_2) - y_w \sin(q_1)\sin(q_2) - z_w \cos(q_2) \tag{3.16}$$

$$M_3 = x_w \sin(q_1) + y_w \cos(q_2) \tag{3.17}$$

It should be noted that although multiple solutions could arise, they are eliminated by violating the human joint limitations.

In order to solve for q_5-q_7, we can articulate the inverse kinematics problem into two sub-problems. After solving the inverse kinematics for q_1 to q_4, we can compute the transformation matrix from the base frame to the wrist frame, $\mathbf{T_4^0}(q_1, q_2, q_3, q_4)$. Then, the transformation matrix from the wrist frame to the end-effector frame can be computed as

$$\mathbf{T_7^4}(q_5, q_6, q_7) = \begin{bmatrix} n_x^{(4)} & s_x^{(4)} & a_x^{(4)} & p_x^{(4)} \\ n_y^{(4)} & s_y^{(4)} & a_y^{(4)} & p_y^{(4)} \\ n_z^{(4)} & s_z^{(4)} & a_z^{(4)} & p_z^{(4)} \\ 0 & 0 & 0 & 1 \end{bmatrix} = \left(\mathbf{T_4^0}\right)^T \mathbf{T} \tag{3.18}$$

where $\mathbf{n^{(4)}} = \begin{bmatrix} n_x^{(4)} & n_y^{(4)} & n_z^{(4)} \end{bmatrix}^T$, $\mathbf{s^{(4)}} = \begin{bmatrix} s_x^{(4)} & s_y^{(4)} & s_z^{(4)} \end{bmatrix}^T$, $\mathbf{a^{(4)}} = \begin{bmatrix} a_x^{(4)} & a_y^{(4)} & a_z^{(4)} \end{bmatrix}^T$ are the orientation vectors and $\mathbf{p^{(4)}} = \begin{bmatrix} p_x^{(4)} & p_y^{(4)} & p_z^{(4)} \end{bmatrix}^T$ is the position vector of the end-effector reference system with respect to the one at the wrist. Since $\mathbf{T_7^4}(q_5, q_6, q_7)$ is known, the joint angles q_5, q_6, q_7 can be computed using Eq. 3.18. The analytical solution is given by:

$$q_5 = arctan2(a_y^{(4)}, a_x^{(4)}) \tag{3.19}$$

$$q_6 = arctan2(\sqrt{\left(a_y^{(4)}\right)^2 + \left(a_x^{(4)}\right)^2}, a_z^{(4)}) \tag{3.20}$$

$$q_7 = arctan2(n_z^{(4)}, -s_z^{(4)}) \tag{3.21}$$

for $q_5 \in [0, \pi)$, and

$$q_5 = arctan2(-a_y^{(4)}, -a_x^{(4)}) \tag{3.22}$$

$$q_6 = arctan2(-\sqrt{(a_y^{(4)})^2 + (a_x^{(4)})^2}, a_z^{(4)}) \tag{3.23}$$

$$q_7 = arctan2(-n_z^{(4)}, s_z^{(4)}) \tag{3.24}$$

for $q_5 \in (-\pi, 0)$.

3.7 Experimental Set-up

Introduction

The subjects were seated on a chair with a distance avoiding a full stretch of the arm (singular configuration). The subjects faced the table and their body were positioned such that the table and the subjects' body center lines were aligned. An active motion capture system was used to track the motion of the arm, as well as compute the human arm configuration. A reference system was defined at the shoulder of the human subject $\langle X, Y, Z \rangle$. It is defined so that the subjects torso coincides with the $X - Z$ plane as shown in Fig. 3.5.

Experimental Protocol

Three right-handed healthy subjects (two males and one female) participated in the experiment. The protocols were approved by the Office of Research Integrity and Assurance, Arizona State University. As explained above, each subject was tested in a sitting posture with his/her torso restrained from torsional movements. Six types of experimental tasks were selected from activities of daily living: (Type 1) arm reaching and pointing, (Type 2) placing a water bottle in discrete locations, (Type 3) placing a small ball in discrete locations, (Type 4) eating, (Type 5) face and head touching and (Type 6) writing. These tasks are chosen based on the basic Activities of Daily Life (ADLs) and each task lasted 20 seconds. No initial information of the configuration of the human arm and the robot arm is

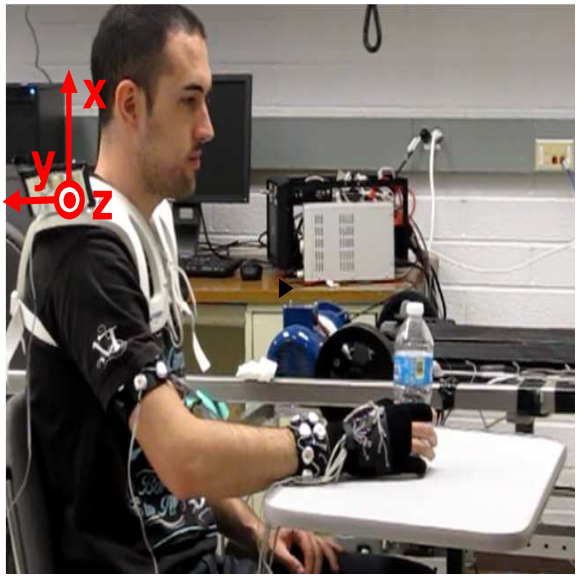

Figure 3.5: Experimental setup: The subjects were seated on a chair with a distance avoiding a full stretch of the arm. An active motion capture system was placed on the right side of the subjects. Position tracking sensors were put on the subjects' shoulder, upper arm, forearm and palm.

needed. In Type 1 task, the subjects were asked to move in the shape of a spiral in order to exam all possible reaching movements. In Type 2 and Type 3 tasks, the subjects grasped the objects with the orientation of the wrist up to subjects' discretion. The two objects were selected to see the effect of the wrist orientation on the swivel angle during object manipulations. Given the ball geometry, it has a negligible effect on the wrist orientation as opposed to the water bottle that dictates a specific final orientation. In Type 4 task, the subject grasped food from discrete locations and put it into their mouth. In Type 5 task, the subject touched discrete locations on his or her head and face continuously. In Type 6 task, the subject wrote on a piece of paper and he/she was asked to write big enough in order to avoid moving his/her wrist only.

Data Collection

The kinematic data of the human arm were collected using an active motion capture system. Markers were put on the rigid bodies of upper arm, forearm and palm respectively in order to calculate the centers of rotation. In order to estimate the biological joint centers shoulder,

elbow and wrist, a calibration experiment was used which required the human subject to attempt to move all joints simultaneously while capturing the position sensor data from the suit of markers and the position of the biological centers with respect to the rigid body that precedes the kinematic chain of the arm was estimated with a least squares method. Having the 3D position of the wrist and elbow, as well as the 3D position and orientation of the rigid body of the palm, a unique solution to the inverse kinematic problem can be found and therefore the 7 joint angles of the upper limb can be obtained.

Chapter 4

DATA ANALYSIS AND RESULTS

4.1 Data Processing

As explained earlier, the goal of the study is to define anthropomorphism in robot motion and drive robot to anthropomorphic configurations. The linear relationship between the intrinsic and extrinsic coordinates are validated and then applied to estimate the swivel angle of the robot arm for an anthropomorphic configuration. Given the elbow and wrist position of the human subjects, we can solve for the actual orientation angles of the upper arm and the forearm with Eq. 2.10, 2.11, 2.12, 3.4, 3.5, 3.6. The spherical coordinates of the wrist position can be computed using Eq. 2.13, 2.14, 2.15. Assume the linear relationship between the intrinsic and extrinsic coordinates can be expressed as:

$$\theta = a_0 + a_1 R + a_2 \chi + a_3 \psi \tag{4.1}$$

Using the least squares approach, the minimum of the function

$$S(a_0, a_1, a_2, a_3) = \sum_{1}^{k} (\theta_a(i) - (a_0 + a_1 R_i + a_2 \chi_i + a_3 \psi_i))^2 \tag{4.2}$$

Where $\theta_a(i)$ is the actual elevation of the upper arm; R, χ and ψ are the radial distance, azimuth, and elevation of the wrist; $k = 0, 1, 2, 3, \cdots$.

Function S measures the sum across trials of the difference between the measured value of θ and the value predicted by the linear model. To minimize S, the best linear model to fit the data can be obtained. The same thing was done to η, β and α. The combined linear relation between the wrist position and the orientation angles across all tasks and subjects is shown in Fig. 4.1. In addition, the statistics are given in Table 4.1. It can be seen that the results are similar to Soechting's results. Here it is needed to emphasize that there was only one simple pointing task in Soechting's experiment while 6 types of more complicated tasks had been conducted in this research. Fig. 4.2 shows the correlation coefficient (r^2) across all subjects and tasks. Due to the arm length difference of the human subjects, the

Table 4.1: Linear relationship between the intrinsic and extrinsic coordinates

i	$OrientationAngle$	$LinearFunction$	r^2
1	θ	$0.2678R+0.5735\psi+66.46$	0.80
2	η	$-0.1516R+1.052\chi+80.51$	0.91
3	α	$0.3248R+0.9347\chi-154.7$	0.95
4	β	$0.1471R-0.981\psi+24.49$	0.92

parameters in the linear relationship will slightly differ from subjects as well as the value of r^2. Tables 4.2, 4.3 and 4.4 show the linear relationship for each subject for all tasks. As shown in Table 4.2, 4.3 and 4.4 the difference in the parameters for the linear relationship is not significant. Comparing the coefficient determination for each type of tasks from Fig. 4.2, there is relatively little difference of residual (r^2). The correlation coefficients on the same task are very similar across subjects, however, for particular orientation angles, the coefficients can differ across tasks. For Type 1 task, the correlation coefficients for all subjects and orientation angles (θ, η, α, β) are close to one and the mean value of r^2 is 0.95. As the tasks get more complicated, the relationship becomes more nonlinear. For Type 2, 3, 4, 6 tasks, the mean value of r^2 of the elevation angles (θ and β) decreased to 0.75. For Type 5 task, its correlation coefficient of the yaw angles (η, α) dropped more significantly to 0.65. This indicates that the subjects share similar correlations for each task while the task difference has more significant affect on the linear relationship and because of the difference in the involvement of each part of the arm, the affect will differ from task to task. Also, by comparing Type 2 and Type 3 tasks, their correlation coefficients are very close implying that hand orientation caused by the different types of object did not affect the linearity.

4.2 Method Evaluation

The proposed method was used in order to control a robot arm (LWR4+, KUKA) to reach the desired position and orientation which was identical to that of the human subject during each trial. For the performance estimation, the mean and standard deviation of the absolute

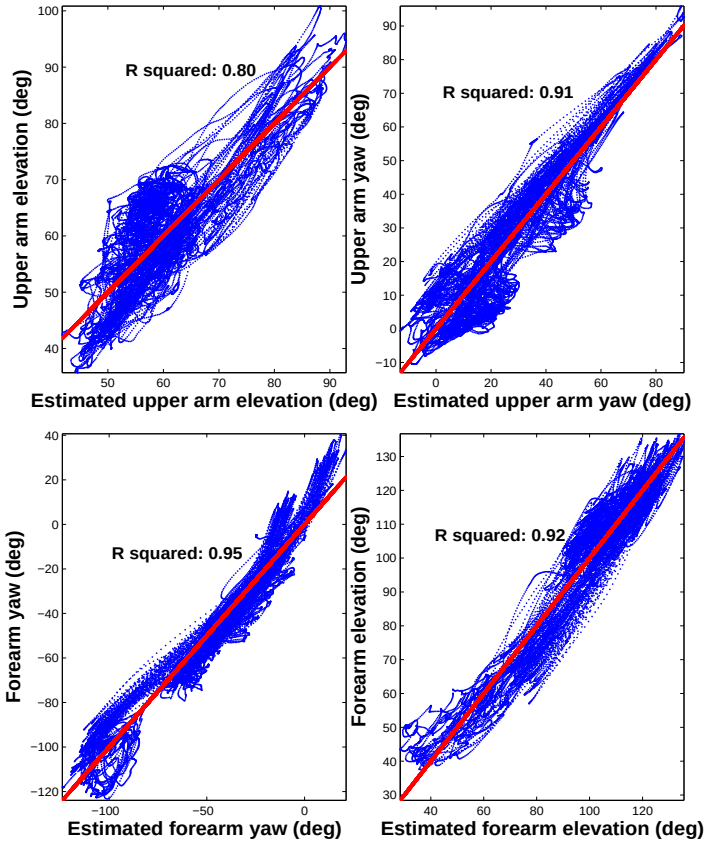

Figure 4.1: Dependence of intrinsic coordinates on extrinsic parameters across all tasks and subjects. The y axis represents the actual orientation angles and the x axis represents estimated value from the the linear combination of target parameters which gave the best fit to the data.

difference between the measured swivel angle collected from the subjects during the experiments and the estimated swivel angle of the robot arm based on the proposed criterion are calculated. The performance estimation results are plotted on all tasks and subjects. Figures 4.3, 4.4, 4.5, 4.6, 4.7, 4.8 show the comparison of the human and the robot arm swivel angles for Type 1 to Type 6 tasks, respectively. The periodic nature of these plots are due to the multiple repetitions of the same task. It should be noted that the peaks in each plot were pauses between the previous and the next movement. In Fig. 4.9, a Graphical Analysis of the data indicates that the mean errors vary from different types of tasks. It should be

Table 4.2: Linear relationship between the intrinsic and extrinsic coordinates for Subject 1

i	$OrientationAngle$	$LinearFunction$	r^2
1	θ	$0.0250R+0.5974\psi+68$	0.82
2	η	$-0.1542R+0.5796\chi+80.81$	0.91
3	α	$0.3318R+0.9974\chi-157.6$	0.95
4	β	$0.1328R-0.9441\psi+31.01$	0.93

Table 4.3: Linear relationship between the intrinsic and extrinsic coordinates for Subject 2

i	$OrientationAngle$	$LinearFunction$	r^2
1	θ	$0.03015R+0.5796\psi+65.57$	0.80
2	η	$-0.1406R+1.036\chi+77.61$	0.91
3	α	$0.3132R+0.9163\chi-151.1$	0.95
4	β	$0.1597R-0.9784\psi+20.51$	0.93

Table 4.4: Linear relationship between the intrinsic and extrinsic coordinates for Subject 3

i	$OrientationAngle$	$LinearFunction$	r^2
1	θ	$0.02495R+0.5266\psi+65.39$	0.78
2	η	$-0.157R+1.049\chi+82.15$	0.90
3	α	$0.3176R+0.8887\chi-154.6$	0.94
4	β	$0.149R+1.054\psi+20.99$	0.92

noted that due to the length difference from the end effector to the wrist, the wrist position of the robot arm will be slightly different from that of the human arm which will cause some errors in the estimation of the swivel angle. Also, there is no initial information for the configuration of the human and robot arm but the estimation results are still very close to the actual swivel angles with 13° mean error across all tasks and subjects. Comparing the results for Type 2 and Type 3 tasks, it implies that the hand orientation caused by the different types of object does not have significant affect on the estimation results which matches the results of the orientation angles shown in Fig. 4.2.

In order to show that the swivel angle is indeed a possible metric of anthropomor-

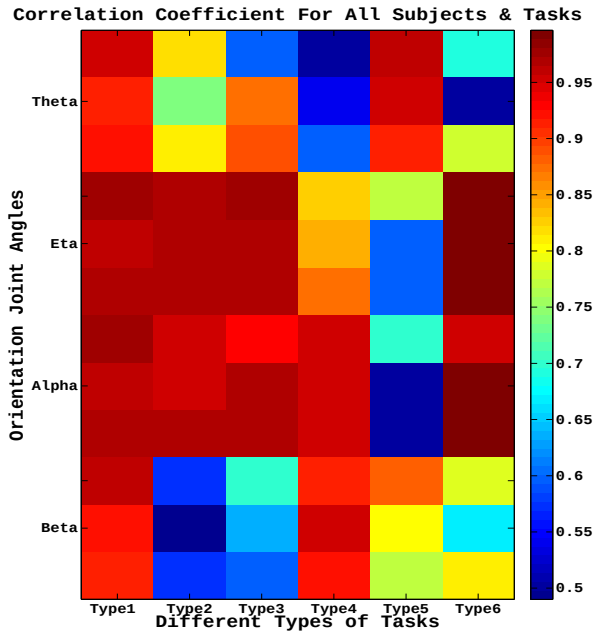

Figure 4.2: Correlation Coefficient Matrix for all subjects and tasks. For each orientation angle, from θ to β, three rows represent three subjects' data respectively. X axis represents the number of the task type. Similar pattern of values was observed across subjects.

phism, we tried to compare the human and robot arm configurations during the tested tasks. These are shown in Fig. 4.10. It must be noted that the joint angles of the human and robot arm will be different due to the difference in the link lengths of the two. Despite this, the robot arm configurations are very similar to the ones of the human, proving that the swivel angle is representative of anthropomorphism in robot motions.

.

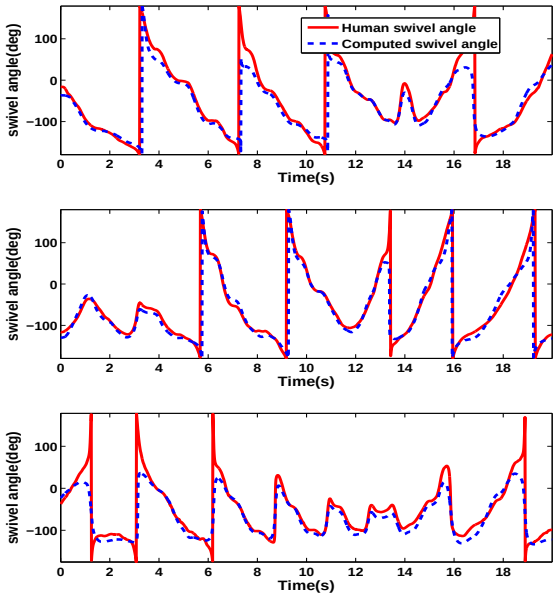

Figure 4.3: Comparison between the robot (computed) swivel angle (dotted line) and the human (measured) swivel angle (solid line) for Type 1 task across all subjects. Each row is from subject 1,2,3, respectively.

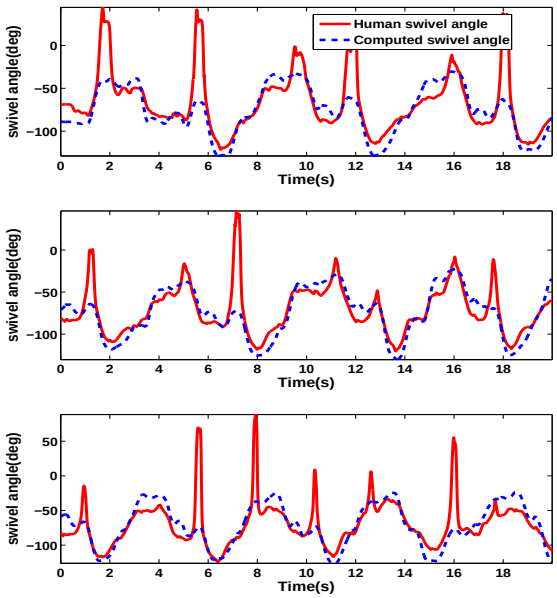

Figure 4.4: Comparison between the robot (computed) swivel angle (dotted line) and the human (measured) swivel angle (solid line) for Type 2 task across all subjects. Each row is from subject 1,2,3, respectively.

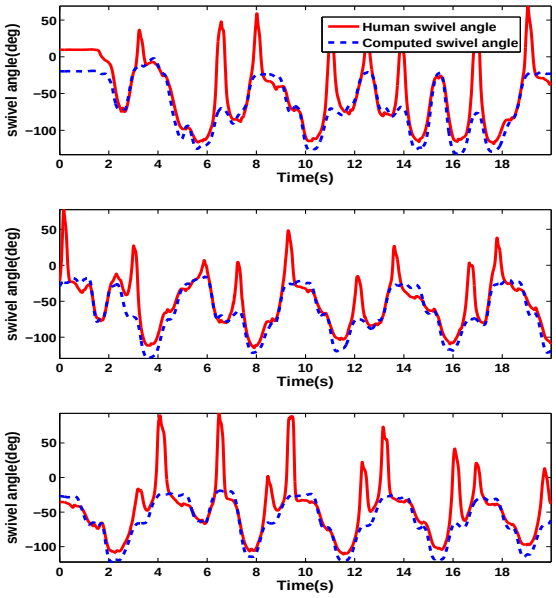

Figure 4.5: Comparison between the robot (computed) swivel angle (dotted line) and the human (measured) swivel angle (solid line) for Type 3 task across all subjects. Each row is from subject 1,2,3, respectively.

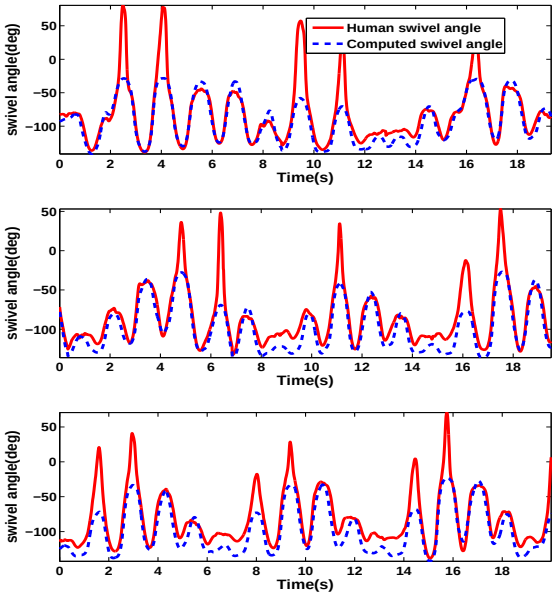

Figure 4.6: Comparison between the robot (computed) swivel angle (dotted line) and the human (measured) swivel angle (solid line) for Type 4 task across all subjects. Each row is from subject 1,2,3, respectively.

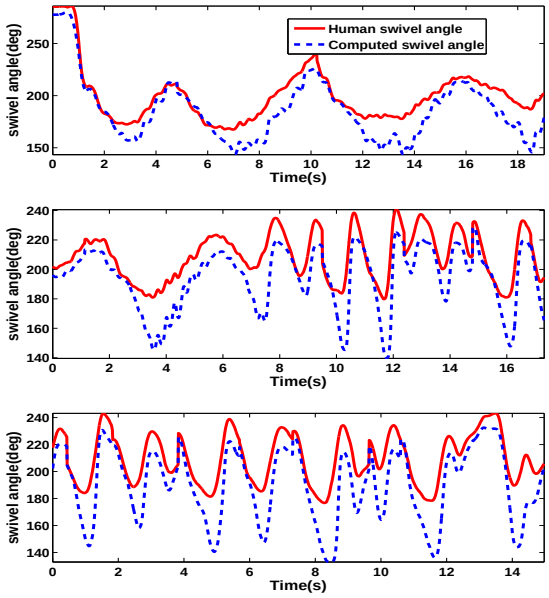

Figure 4.7: Comparison between the robot (computed) swivel angle (dotted line) and the human (measured) swivel angle (solid line) for Type 5 task across all subjects. Each row is from subject 1,2,3, respectively.

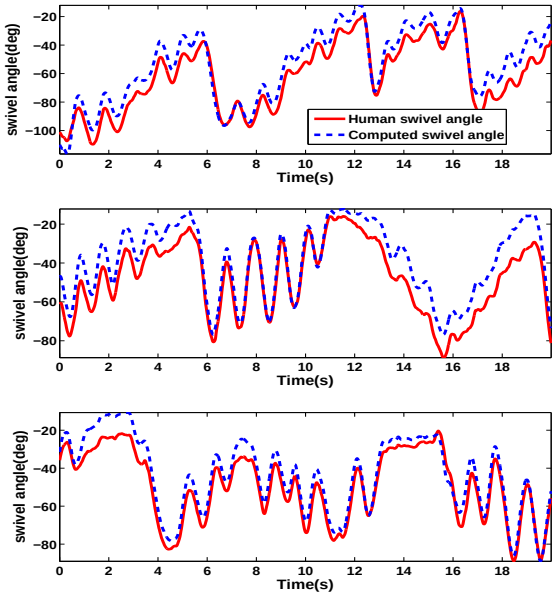

Figure 4.8: Comparison between the robot (computed) swivel angle (dotted line) and the human (measured) swivel angle (solid line) for Type 6 task across all subjects. Each row is from subject 1,2,3, respectively.

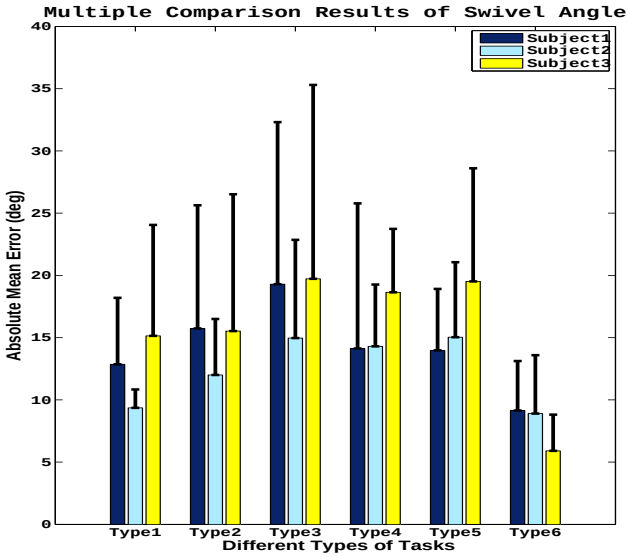

Figure 4.9: The mean error with associated standard deviation (one sided) of the swivel angle from the combined linear model (ϕ) with respect to types of tasks.

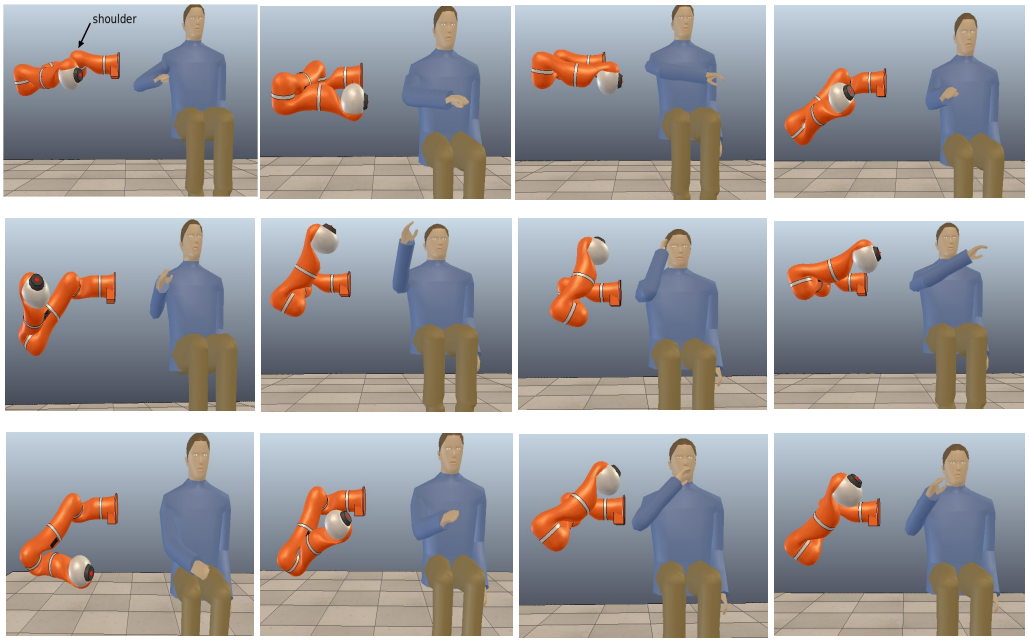

Figure 4.10: Snapshots of the human arm performing 3D motions and the robot arm driven by the proposed method.

Chapter 5

DISCUSSIONS

In this thesis we consider the problem of generating human-like motions from the kinematic point of view, taking into account data recorded during a wide variety of everyday life tasks. We use findings from neurophysiology that note the importance of the elbow position and orientation in anthropomorphic arm movements. The swivel angle of the elbow is used as a human arm motion parameter for the robot arm to mimic. Using experimental data recorded from a human subject during every-day life tasks, we validate the linear relations between intrinsic and extrinsic coordinates that estimates the swivel angle, given the desired end-effector position. Requiring a desired swivel angle simplifies the kinematic redundancy of the robot arm.

As shown in **Chapter 4**, there is a linear relationship between the intrinsic and extrinsic coordinates across all subjects, and the parameters of the linear relationship will vary slightly due to the arm length difference. The complexity of the task has some minor affect on the linearity. However, the mean value of correlation coefficients of all orientation joint angles is 0.9, indicating that the linearity still plays an important role in the human arm motion. As shown in Fig. 4.9, the estimation results are very close to the actual swivel angles with 13° mean error across all tasks and subjects, again with no initial information for the configuration of the human and robot arm. Fig. 4.10 also shows that the swivel angle can be used as a metric of anthropomorphism.

5.1 Conclusion

The proposed method is tested with an anthropomorphic redundant robot arm and the computed motion profiles are compared to the ones of the human subject. It is shown that the method computes anthropomorphic configurations for the robot arm, even if the robot arm has different link lengths than the human arm, or starts its motion from random configurations. This can be useful in a wide range of robot arms that interface with humans and

are operated in human-cluttered environments. Especially in humanoid robots, the method can be directly used in order to obtain anthropomorphic arm motions, while it can be easily extended to dual arm configurations, describing the joint angle dependencies in dual arm robotic systems. The novelty of the proposed method can be found in two main points. First, the method uses the concept that the positioning of the elbow joint is a decisive factor of anthropomorphic configurations in humans. Based on that, we define the swivel angle and design our inverse kinematic problem in order to provide similar (but not identical) robot swivel angles with those of the human during every-day life tasks. This results in an analytic closed-form solution of the inverse kinematic problem. Secondly, the method is generalizable, since it can be used in a wide variety of redundant robot arms, as long as an elbow-equivalent point is defined on the robot arm.

5.2 Future Work

While this control scheme solves many aspects of current difficulties in robotic interaction, it needs further investigation to characterize all types of human motion. While the idea of manipulation is integral to human motion, other considerations are pertinent, such as force. More experimentation and observation is required to develop a more robust control system for the manipulator to interact with humans in every-day life. This development requires not only a kinematic analysis of human motion but one which is driven by end effector forces and torques or motion impedances. Only upon the combination of all these considerations will a truly generalizable, anthropomorphic manipulator evolve.

REFERENCES

[1] PanagiotisK. Artemiadis, PantelisT. Katsiaris, and KostasJ. Kyriakopoulos. A biomimetic approach to inverse kinematics for a redundant robot arm. *Autonomous Robots*, 29(3-4):293–308, 2010. 2, 8

[2] T. Asfour and R. Dillmann. Human-like motion of a humanoid robot arm based on a closed-form solution of the inverse kinematics problem. In *Intelligent Robots and Systems, 2003. (IROS 2003). Proceedings. 2003 IEEE/RSJ International Conference on*, volume 2, pages 1407–1412 vol.2, 2003. 2, 22

[3] Vittorio Caggiano, Agostino De Santis, Bruno Siciliano, and Angelo Chianese. A biomimetic approach to mobility distribution for a human-like redundant arm. In *Biomedical Robotics and Biomechatronics, 2006. BioRob 2006. The First IEEE/RAS-EMBS International Conference on*, pages 393–398. IEEE, 2006. 2

[4] Holk Cruse, Erhard Wischmeyer, Michael Brüwer, Peter Brockfeld, and A Dress. On the cost functions for the control of the human arm movement. *Biological Cybernetics*, 62(6):519–528, 1990. 1, 2

[5] Holk Cruse, Erhard Wischmeyer, Michael Brüwer, Peter Brockfeld, and A Dress. On the cost functions for the control of the human arm movement. *Biological Cybernetics*, 62(6):519–528, 1990. 8

[6] Filiep Debaere, Nicole Wenderoth, Stefan Sunaert, Paul Van Hecke, and SP Swinnen. Cerebellar and premotor function in bimanual coordination: parametric neural responses to spatiotemporal complexity and cycling frequency. *Neuroimage*, 21(4):1416–1427, 2004. 2

[7] A. Edsinger and C.C. Kemp. Human-robot interaction for cooperative manipulation: Handing objects to one another. In *Robot and Human interactive Communication, 2007. RO-MAN 2007. The 16th IEEE International Symposium on*, pages 1167–1172, 2007. 2, 8, 19

[8] Kenneth N Groom, Anthony A Maciejewski, and Venkataramanan Balakrishnan. Real-time failure-tolerant control of kinematically redundant manipulators. *Robotics and Automation, IEEE Transactions on*, 15(6):1109–1115, 1999. 5

[9] Neville Hogan. An organizing principle for a class of voluntary movements. *The Journal of Neuroscience*, 4(11):2745–2754, 1984. 2

[10] J.M. Hollerbach and Ki Suh. Redundancy resolution of manipulators through torque optimization. *Robotics and Automation, IEEE Journal of*, 3(4):308–316, 1987. 2

[11] JOHNM Hollerbach and Ki Suh. Redundancy resolution of manipulators through torque optimization. *Robotics and Automation, IEEE Journal of*, 3(4):308–316, 1987. 5, 6

[12] O. Khatib and J. Burdick. Motion and force control of robot manipulators. In *Robotics and Automation. Proceedings. 1986 IEEE International Conference on*, volume 3, pages 1381–1386, 1986. 2

[13] ChangHwan Kim, Doik Kim, and Yonghwan Oh. Solving an inverse kinematics problem for a humanoid robot2019s imitation of human motions using optimization. In *ICINCO'05*, pages 85–92, 2005. 2, 7

[14] Hyunchul Kim, L.M. Miller, A. Al-Refai, M. Brand, and J. Rosen. Redundancy resolution of a human arm for controlling a seven dof wearable robotic system. In *Engineering in Medicine and Biology Society,EMBC, 2011 Annual International Conference of the IEEE*, pages 3471–3474, 2011. 3, 18

[15] Hyunchul Kim, L.M. Miller, N. Byl, G. Abrams, and J. Rosen. Redundancy resolution of the human arm and an upper limb exoskeleton. *Biomedical Engineering, IEEE Transactions on*, 59(6):1770–1779, 2012. vi, 3, 8, 11, 12, 14, 18, 22, 23

[16] James U Korein. *A geometric investigation of reach*. MIT press, 1986. 8, 19

[17] Mark L Latash. Control of human movement. 1993. 2

[18] David C Lay. Linear algebra and its applications. *Univ. of Maryland-College Park*, 2003. 11

[19] Alain Liegeois. Automatic supervisory control of the configuration and behavior of multibody mechanisms. *IEEE Transactions on Systems, Man, and Cybernetics*, 7(12):868–871, 1977. 1, 5, 6

[20] Anthony A Maciejewski. Dealing with the ill-conditioned equations of motion for articulated figures. *Computer Graphics and Applications, IEEE*, 10(3):63–71, 1990. 11

[21] Anthony A Maciejewski and Charles A Klein. Obstacle avoidance for kinematically redundant manipulators in dynamically varying environments. *The international journal of robotics research*, 4(3):109–117, 1985. 1, 5, 6

[22] Levi Makaio Miller, Hyunchul Kim, and Jacob Rosen. Redundancy and joint limits of a seven degree of freedom upper limb exoskeleton. *Conf Proc IEEE Eng Med Biol Soc*, 2011:8154–7, 2011. 3, 18

[23] Yoshihiko Nakamura. Inverse kinematic solutions with singularity robustness for robot manipulator control. *J. of Dynamic Systems, Mes. and Contr.*, 108:163–171, 1986. 1

[24] Nancy Pollard, Jessica K Hodgins, M.J. Riley, and Chris Atkeson. Adapting human motion for the control of a humanoid robot. In *Proceedings of the IEEE International Conference on Robotics and Automation (ICRA '02)*, May 2002. 2, 7

[25] Veljko Potkonjak. Distributed positioning for redundant robotic systems. *Robotica*, 8(1):61–67, 1990. 5

[26] Veljko Potkonjak, Dragan Kostic, Spyros Tzafestas, Mirjana Popovic, Mihajlo Lazarevic, and Goran Djordjevic. Human-like behavior of robot arms: general considerations and the handwriting taskpart ii: the robot arm in handwriting. *Robotics and Computer-Integrated Manufacturing*, 17(4):317 – 327, 2001. 7

[27] Veljko Potkonjak, Mirjana Popovic, Mihailo Lazarevic, and Jelena Sinanovic. Redundancy problem in writing: from human to anthropomorphic robot arm. *Systems, Man, and Cybernetics, Part B: Cybernetics, IEEE Transactions on*, 28(6):790–805, 1998. 1

[28] Veljko Potkonjak, Spyros Tzafestas, Dragan Kostic, and Goran Djordjevic. Human-like behavior of robot arms: general considerations and the handwriting taskpart i: mathematical description of human-like motion: distributed positioning and virtual fatigue. *Robotics and Computer-Integrated Manufacturing*, 17(4):305 – 315, 2001. 1, 2, 5, 7

[29] Lorenzo Sciavicco and Bruno Siciliano. *Modeling and control of robot manipulators*. McGraw-Hill, 1996. 19, 20, 22

[30] AH Sief-Naraghi and JM Winters. Changes in musculoskeletal control strategies with loading: inertial, isotonic, random. In *ASME Biomech. Symp*, pages 355–358, 1989. 2

[31] JF Soechting. Does position sense at the elbow reflect a sense of elbow joint angle or one of limb orientation? *Brain research*, 248(2):392–395, 1982. 17

[32] JF Soechting and B Ross. Psychophysical determination of coordinate representation of human arm orientation. *Neuroscience*, 13(2):595–604, 1984. 17

[33] John F Soechting and Martha Flanders. Errors in pointing are due to approximations in sensorimotor transformations. *Journal of Neurophysiology*, 62(2):595–608, 1989. v, 13, 16, 18

[34] John F Soechting and Martha Flanders. Sensorimotor representations for pointing to targets in three-dimensional space. *Journal of Neurophysiology*, 62(2):582–594, 1989. vii, 13, 15, 16, 18

[35] John F Soechting and Martha Flanders. Sensorimotor representations for pointing to targets in three-dimensional space. *Journal of Neurophysiology*, 62(2):582–594, 1989. 14

[36] JJ Temprado, SP Swinnen, Richard G Carson, A Tourment, and M Laurent. Interaction of directional, neuromuscular and egocentric constraints on the stability of preferred bimanual coordination patterns. *Human Movement Science*, 22(3):339–363, 2003. 2

[37] Deepak Tolani, Ambarish Goswami, and Norman I. Badler. Real-time inverse kinematics techniques for anthropomorphic limbs. *Graphical Models*, 62(5):353 – 388, 2000. 8, 18, 22

[38] Ales Ude, Curtis Man, Marcia Riley, and Christopher G Atkeson. Automatic generation of kinematic models for the conversion of human motion capture data into humanoid robot motion. 2000. 2

[39] CJ Worringham, GE Stelmach, and ZE Martin. Limb segment inclination sense in proprioception. *Experimental Brain Research*, 66(3):653–658, 1987. 17

[40] Tsuneo Yoshikawa. Robotics research: Can robots have human-level manipulation skill. http://www.kyoto-u.ac.jp/en/research/forefront/message/rakuyu06_a.htm. vi, 8, 9

[41] Tsuneo Yoshikawa. Manipulability of robotic mechanisms. *The international journal of Robotics Research*, 4(2):3–9, 1985. 5

[42] A Zagorianos, E Kontoyannis, and S Tzafestas. Resolved motion model based predictive control of redundant robots. *Mathematics and computers in simulation*, 37(2):195–205, 1994. 5